DEFORMATION MONITORING AND SENSITIVITY ANALYSIS OF UNDER-CONSTRUCTION BRIDGES CONSIDERING PS OPTIMIZATION

Zidong Xu [1], Xuedong Zhang [1,2*], Haoyun Xie[1], Bo Chen [1], Zhaowen Li [1], Yaqi Zhang [1]

1 Beijing University of Civil Engineering and Architecture, 102616, Beijing, China, 2108570021124@stu.bucea.edu.cn
2 Beijing Key Laboratory of Urban Spatial Information Engineering, 100038, Beijing, China,

*Corresponding author.
E-mail addresses: zhangxuedong@bucea.edu.cn (X.Z.)

KEY WORDS: Under-construction Bridge, PS identification, Statistical median of Amplitude mean, Deformation characteristics, Temperature.

ABSTRACT:

During the construction and operation of bridges, safety accidents can occur due to improper design, construction, development of structural diseases, and inadequate maintenance measures. Such incidents can lead to significant property damage and casualties. InSAR technology is increasingly playing a critical role in the deformation monitoring of linear projects, such as bridges and roads because it is not affected by light and weather conditions. However, in the process of bridge construction, the instability of the environment often results in low scattering intensity, which can make it challenging to obtain a sufficient number of permanent scatterer (PS) points. This study proposes a method to optimize the identification of PS points by combining amplitude dispersion index, statistical median of amplitude mean, and temporal coherence coefficient, based on TerraSAR-X data. We then employed PS-InSAR technology to monitor the deformation of the under-construction bridge over the JingXiong Expressway-Yongding River, China. Furthermore, we conducted temporal subsidence analysis for different structural locations of the bridge while combining temperature data from weather stations to carry out a sensitivity analysis of the bridge deformation. The study results demonstrated that (1) the proposed method for optimizing the identification of PS points outperformed the two traditional methods in terms of increasing the selection of PS candidates by 14% and 10% respectively, while also leading to better quality identification of the PS candidates; (2) the main body of the under-construction bridge appeared relatively stable at present, with the deformation of the bored cast-in-situ piles and the connection of the approach span and abutment showing greater magnitude compared to other areas. Thus, it is essential to conduct regular monitoring of these regions and implement preventive measures in the future; and (3) the deformation of the under-construction bridge is correlated with the ambient temperature, and different structural locations display varying sensitivity to temperature changes. The findings of this study can help guide the subsequent construction and safe operation of the under-construction bridge after completion.

1. INTRODUCTION

During the construction and operation of bridges, various safety accidents may occur due to human awareness limitations, improper design and construction, structural disease development, and inadequate reinforcement and maintenance measures. Such catastrophic incidents can result in significant property damage and casualties (Galvão et al.2021). InSAR technology, which is not affected by light and weather conditions, can address the limitations of traditional deformation monitoring methods, such as limited measurement range, short measurement distance, sensitivity to environmental influences, and excessive workload. Consequently, InSAR technology is increasingly acquiring a vital role in the high-precision, rapid, and long-term deformation monitoring of linear projects, such as roads and bridges (Ge et al.2016; Cusson et al.2018). For under-construction bridges, the low scattering intensity of the bridge caused by the unstable environment makes it challenging to obtain a sufficient number of reliable permanent scatterer (PS) points, hampering the monitoring process (Farneti et al. 2023). Therefore, it is of great significance and application value to study the PS point recognition method suitable for under-construction bridges and carry out the time series deformation monitoring of under-construction bridges during the construction of under-construction bridges and subsequent safe operation.

For PS point selection, Ferretti et al. proposed a PS identification and selection algorithm that included the amplitude dispersion index threshold method, time-dependent threshold method, and phase dispersion threshold method, and conducted corresponding experimental studies for PS point selection (Ferretti et al.2000; Ferretti et al.2001). Sankarambadi et al. employed a random matrix theory approach to study the covariance matrix to identify the statistical properties of the eigenvalues of both simulated and real SAR data (Navneet et al.2017). A pixel selection strategy based on the highest eigenvalue threshold of the coherence matrix is used to distinguish low coherent or noisy pixels. Zhou et al.proposed a joint modeling of the PS-InSAR technique and SAR laminar imaging RELAX algorithm to identify single and double scatterers, which enhances the identification and reliability of PSs(Zhou et al.2020). Pierluigi et al.monitored landslides in the hamlet of Papanice, Crotone, southern Italy using Coherent Pixel Technique-Temporal Sublook Coherence (CPT-TSC) and Small Baseline Subset (SBAS) techniques. The result showed that the higher density of targets identified through CPT-TSC enabled us to analyze in detail the slope behavior in order to design possible mitigation interventions(Pierluigi et al.2017). Although the aforementioned study provides a significant reference value for the identification and selection of PS points for under-construction bridges, it is still challenging to obtain dense and accurate PS points for such bridges due to the

instability of the environment and the low intensity of backscattering caused by construction shocks.

Numerous experts and scholars have conducted research on the deformation monitoring of completed linear projects and obtained significant results, providing valuable insights for the preliminary study of deformation monitoring of under-construction bridges. For instance, Lazecky and colleagues investigated the deformation of three bridges in Bratislava, Ostrava, and Hong Kong using the PS-InSAR technique and analyzed the effect of thermal expansion on structural deformation (Lazecky et al.2015). Schlögl et al. proposed the use of PS-InSAR for monitoring Vienna Harbor bridges (Schlögl et al.2021). By analyzing and refining the raw time series, vertical and horizontal deformation components were extracted. Furthermore, the seasonal trend of deformation was decomposed by incorporating temperature data. Lyu et al. employed the PSI technique to analyze the surface deformation time series of 25 highway overpasses in Beijing (Lyu et al.2021). They proposed Deformation Concentration Degree (DCD) and Deformation Concentration Period (DCP) indices to explore seasonal deformation. The aforementioned studies primarily focus on identifying and analyzing the structural risks of completed bridges using InSAR technology. However, the vibrations are generated during the bridge construction, and environmental factors can significantly impact bridge structures, leading to potential safety hazards in the later stages of the bridge's lifetime. Thus, this study focuses on an under-construction bridge that connects the JingXiong Expressway to the Yongding River in Beijing, China. We propose a novel method that combines the amplitude dispersion index, a statistical median of amplitude mean, and temporal coherence coefficient to locate PS points and perform temporal subsidence analysis at various structural locations of the bridge. Additionally, we incorporate weather station temperature data to conduct a deformation sensitivity analysis of the under-construction bridge. The findings of this study are expected to provide critical data support and valuable references for the construction and subsequent safety monitoring of under-construction bridges.

2. STUDY AREA AND DATA SOURCE

2.1 Study Area

The Yongding River Bridge, located at the intersection of the Yongding River and JingXiong Expressway in Beijing, China, has a total length of 1.62 kilometers and is designed as a flying arch bridge. The main bridge structure is an arch bridge with a main arch span of 300 meters (including 410 meters for the east approach bridge and 690 meters for the west approach bridge). As the bridge has a large span, complex geological conditions, and high accuracy and safety requirements, it plays a crucial role in the completion of the entire JingXiong Expressway.

During the image acquisition period, the bridge was in the initial stage of construction. Based on the Google Earth satellite map, we observed that a portion of the approach span and abutment had been erected, while the bridge's main body was still under construction. Currently, bored cast-in-situ piles are being built. The study area is shown in Figure 1.

2.2 Data Source

The remote sensing data used in this study are 17 TerraSAR-X images from November 2021 to September 2022, and their basic information is presented in Table 1. Additionally, the data used include Digital Elevation Model (DEM) data and temperature data. The DEM data used in this study are 30m SRTM data obtained from a joint measurement by NASA and the Department of Defense National Mapping Agency (NIMA) (https://srtm.csi.cgiar.org/srtmdata/). Meanwhile, the temperature data are derived from meteorological site data collected from Beijing Capital International Airport, China.

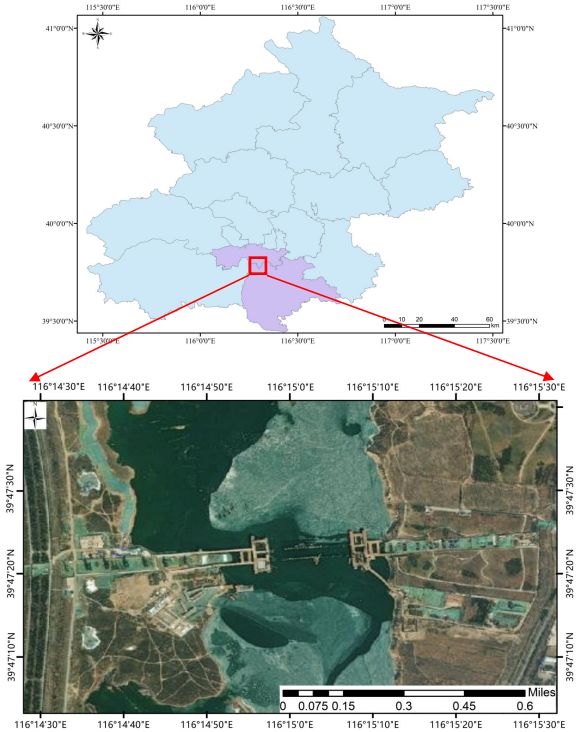

Figure 1. Schematic diagram of the study area.

TerraSAR-X	Date	B_T(day)	$B_\perp$(m)
1	20211113	-142	152.9
2	20211124	-131	84.8
3	20220129	-66	8.2
4	20220220	-44	163.8
5	20220303	-33	161.8
6	20220325	-11	113.6
7	20220405	0	0
8	20220427	22	208.8
9	20220508	33	40.0
10	20220530	55	186.9
11	20220610	66	172.1
12	20220702	88	-3.0
13	20220724	110	-224.7
14	20220804	121	64.7
15	20220815	132	-380.0
16	20220906	154	-337.3
17	20220928	176	-136.0

Table 1. The temporal and perpendicular baselines of the TerraSAR-X dataset.

3. RESEARCH METHODS

To monitor the deformation of the under-construction bridge over the JingXiong Expressway-Yongding River, this study proposes a PS identification method based on the statistical median of amplitude mean (SM), the amplitude dispersion index (ADI), and the coherence coefficient threshold (CCT), using TerraSAR-X images. This method involves obtaining the statistical median of amplitude mean based on the conventional calculation of amplitude dispersion index, and then combining it with the coherence coefficient threshold to identify PS points. The PS points identified by the Three-threshold joint algorithm (TTJA), which combines the ADI, SM, and CCT, are compared with those identified by the traditional method. Deformation estimation and error phase separation are performed to obtain deformation information in the vicinity of the under-construction bridge. The deformation at different positions of the under-construction bridge is analyzed, and sensitivity analysis is carried out at different structural positions of the under-construction bridge, considering temperature data, to investigate the causes of deformation. The specific process is shown in Figure 2.

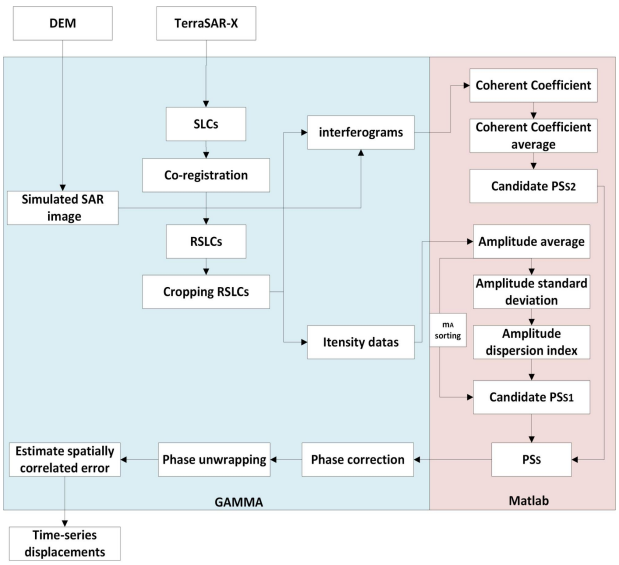

Figure 2. Technical framework for PS points joint selection and timing processing.

3.1 Amplitude Dispersion Index and Statistical Median of Amplitude Mean

Following the alignment of N+1 SLC SAR images, we solve the amplitude value for each image element from the amplitude image, denoted as A;

$$\mathrm{A} = \sqrt{\left[Im\left(s(i,j)\right)\right]^2 + \left[Re\left(s(i,j)\right)\right]^2} \quad (1)$$

For the image element located at row i and column j, the real part is represented by $\mathrm{Im}\left(\mathrm{s(i,j)}\right)$,while the imaginary part is represented by $\mathrm{Re}\left(\mathrm{s(i,j)}\right)$(Luo et al.2007).

The magnitude values of image elements in the SAR images are arranged in a time-sequential manner. Subsequently, a statistical analysis of this sequence is performed to obtain the magnitude mean value, denoted as m_A.

$$m_A = \frac{1}{N+1}\sum_{i=1}^{n} A_i \quad (2)$$

Afterwards, the temporal amplitude standard deviation is calculated based on the mean amplitude value;

$$\sigma_A = \sqrt{\frac{1}{N+1}\sum_{i=0}^{n}(A_i - m_A)^2} \quad (3)$$

The amplitude dispersion index is obtained by dividing the calculated amplitude standard deviation by the mean amplitude value (Liu et al.2020).

$$\mathrm{ADI} = \frac{\sigma_A}{m_A} \quad (4)$$

In the initial stage of screening, a reasonable threshold value for candidate point identification, T_d, is determined based on the amplitude dispersion index. Points with an amplitude dispersion index less than or equal to T_d are identified as PS candidates, while points with an amplitude dispersion index greater than T_d are labeled non-candidates. Following the initial screening, a second screening is conducted to extract the PS candidate points identified in the first phase. During this stage, the mean amplitude of the candidate points is sorted, using the median value of the sequence as the threshold value, and points with mean amplitudes greater than the threshold value are selected as the PS points for the second screening (Luo et al.2018). The PS candidate points obtained via this method are denoted as PS_{S1}.

3.2 Temporal Coherence Coefficient

Assuming that there are N+1 time-series SAR images in the study area, one of them is taken as the master image; all the other images (slaves) are aligned and resampled to match the master image, forming N interferometric pairs by the time axis. Theoretically, the noise level of the interferometric phase calculated from SAR image pairs can be determined by the coherence measure γ. Therefore, acquiring coherence coefficient information from images can serve as a straightforward and effective method for filtering valid PS points (Natsuaki et al., 2018). In the actual calculation, the coherence coefficient γ at a specific resolution unit can be estimated using the information from adjacent pixels within a certain range (window) surrounding the image element, as expressed by:

$$\gamma = \frac{\left|\sum_{i=1}^{m}\sum_{j=1}^{n} S_1(i,j)S_2^*(i,j)\right|}{\sqrt{\sum_{i=1}^{m}\sum_{j=1}^{n}|S_1(i,j)|^2 \sum_{i=1}^{m}\sum_{j=1}^{n}|S_2(i,j)|^2}} \quad (5)$$

In this equation, S1 and S2 represent the local pixel information (in complex form) of the two SAR images that form an interferometric pair, * denotes the complex conjugate operator, and m and n represent the size of the local shift window. Generally, the larger the coherence coefficient γ (γ ∈ [0, 1]), the lower the noise of the interference phase. Assuming the existence of N time-series interferometric image pairs, the temporal coherence coefficients $\gamma_1, \gamma_2, \ldots, \gamma_N$ for any resolution cell in the overlapping area of the images can be obtained from Equation (5). To search for PS points, the average temporal coherence coefficient value is calculated for each pixel as follows:

$$\overline{\gamma} = \frac{1}{N}\sum_{i=1}^{N}\gamma_i \quad (6)$$

Subsequently, a suitable threshold value Tγ is established, and image pixels whose average coherence coefficients are greater than or equal to this threshold (i.e. $\gamma \geqslant \overline{\gamma}$) are identified as PS points. The PS candidate points obtained via this approach are referred to as PS_{S2}.

Generally, a low coherence coefficient threshold is effective in filtering out image elements with significantly low correlation. Through several experimental analyses, a threshold value of 0.15 is deemed suitable for filtering pixels located in regions covered by water bodies and vegetation. The basis for removing water bodies and vegetation is their radar reflection characteristics. The water body is generally a mirror reflection,

and the vegetation reflection is easily affected by external random disturbances (such as vegetation growth, leaf swing with the wind, etc.).

3.3 Amplitude Dispersion Index Statistical Median of Amplitude Mean and Coherence Coefficient Threshold joint PS_S identification

Previous studies have demonstrated that the signal-to-noise ratio (SNR) of interferograms can be estimated using coherence coefficients (Jung et al.2016).

$$\mathrm{SNR} = \frac{\gamma}{1+\gamma} \tag{7}$$

The coherence coefficient γ is directly proportional to the SNR of the interferogram; the higher the coefficient, the greater the SNR, resulting in lower noise levels. Consequently, the magnitude of the coherence coefficient γ can be utilized to differentiate between high and low SNR levels (Jung et al.2016).

Following the aforementioned study, the PS candidate points identified in sections 3.1 and 3.2 are combined;

$$\mathrm{PS} = \mathrm{PS}_{S1} \cup \mathrm{PS}_{S2} \tag{8}$$

Lastly, the jointly-selected PS points are determined based on their interferogram SNR, with PS candidates exhibiting lower noise levels (i.e. higher SNR) being designated as the final PS points.

4. RESULT ANALYSIS

4.1 PS_S Identification Analysis of Under-Construction Bridges

Figure 3 displays the results of the PS candidate points screened using three different identification methods after mask extraction for the main body of the bridge and the extension area of the east-west approach bridge. For this study, the amplitude dispersion index threshold was set to 0.75. The identification results of the ADI method in Fig. 3(a) reveal that the PS points can cover most of the under-construction bridge at JingXiong Expressway-Yongding River, except for the sparse PS point located on the south side bored cast-in-situ piles and on the west side of the abutment bearing. Additionally, some background noise signals and points on the water surface were misclassified as PS points.

Figure 3(a). ADI method PS points identification results

The coherence coefficient threshold was set to 0.45 for this analysis. Based on the identification results of the CCT method in Fig. 3(b), it is evident that the PS points can largely cover the area of the bored cast-in-situ piles and compensate for the point vacancy in the western section of the under-construction abutment bearing. However, the points are distributed in fragments, and the shadow area of the piers in the river is mistakenly identified as PS points. Additionally, only a few points are covered in the construction area of the abutment on the east side.

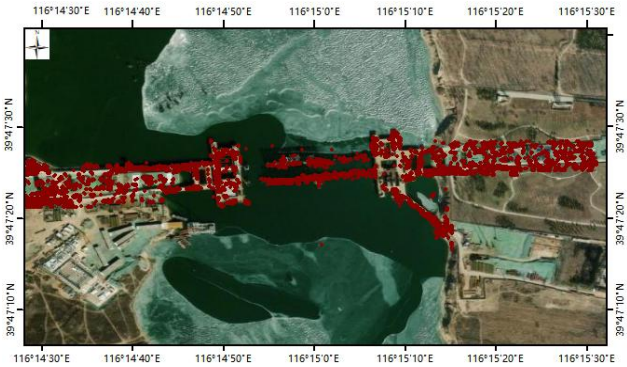

Figure 3(b). CCT method PS points identification results.

After screening the PS candidate points using the amplitude dispersion index threshold, the mean amplitude values of these points are sorted, and the median value is selected for secondary screening. In this study, the calculated median value is 0.62. Based on the identification results of the TTJA method in Fig. 3(c), it is evident that the joint point identification method combines the advantages of amplitude dispersion stability and temporal coherence. The identified PS points can cover not only the main part of the under-construction bridge but also other areas with more uniform point distribution. Moreover, misidentified points in the west area of the bored cast-in-situ piles and the middle section of the north side where there are no pile bodies have been removed. Additionally, some error points such as water body shadows and noise have been eliminated.

According to statistical analysis, the ADI method extracted a total of 7,235 PS candidates along the bridge and the area along the approach span. The CCT method extracted a total of 7,465 PS candidates, while the TTJA method adopted in this study identified a total of 8,243 PS candidates. The number of candidate points increased by 14% compared to the ADI method and 10% compared to the CCT method.

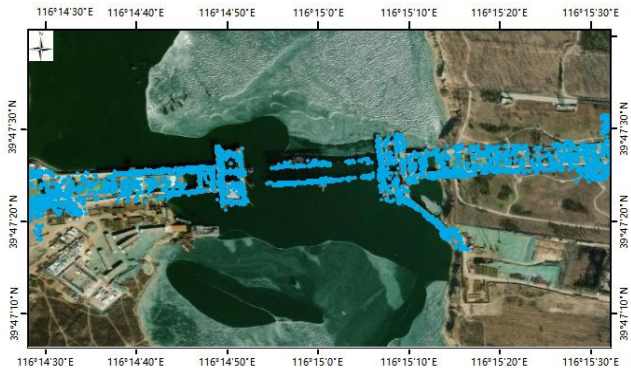

Figure 3(c). TTJA method PS points identification results.

4.2 Deformation Analysis of Under-Construction Bridges

Mask files of the identified PS points were generated for subsequent processing (Delgado et al.2019). The first step was to perform phase unwrapping, followed by the removal of trend error and atmospheric error to obtain the line-of-sight (LOS) deformation rate. Then, the vertical deformation rate was calculated based on the satellite incidence angle to obtain the

deformation trend of the under-construction bridge at JingXiong Expressway-Yongding River and the surrounding area.

As shown in the deformation rate in Figure 4, the subsidence rate of the bridge and the surrounding area during the monitoring period was moderate, with a deformation rate ranging from -15 to 20 mm/year. Overall, the deformation trend showed a western subsidence and an eastern uplift trend. The most significant subsidence occurred in the northwest side of the under-construction bridge and the south side of the riverbank area, with a subsidence rate difference of 5-10 mm/year that radiated to the surrounding area.

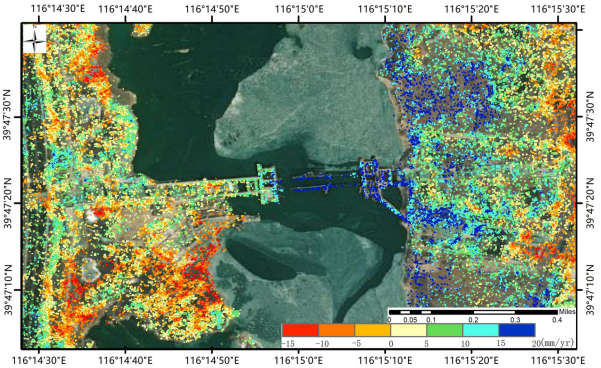

Figure 4. Deformation rate of the under-construction bridge over the Jingxiong Expressway-Yongding River and the surrounding area.

The analysis of the causes of deformation reveals that the bridge over the Yongding River is essentially surrounded by the riverbank area, which is subject to erosion and siltation. This phenomenon can lead to the loosening of the foundation, resulting in subsidence. Secondly, during bridge construction, the use of construction machinery and the transportation of materials can cause impacts and vibrations to the foundation. These activities can somewhat accelerate the subsidence process in the surrounding riparian area.

Concerning the abutment of the under-construction bridge body, the deformation of the west side abutment is slightly smaller than that of the east side. Specifically, most of the west side abutment exhibits a deformation rate ranging from 10-15 mm/year, while the middle and south side of the east side abutment reaches 15-20 mm/year. As for the approach span part, the deformation trend of the west side approach span is not significant, while most of the east side approach span shows a slight uplift. The uplift is more prominent at the beginning of the approach span and the connection with the abutment, with a rate reaching 20 mm/year.

The analysis of the reasons for this phenomenon indicates that differences in the depth and load-bearing capacity of the soil foundation may be the reason. This situation can lead to insufficient load-bearing capacity at the beginning of the under-construction approach span and the connection with the abutment, resulting in an uplift. The bored cast-in-situ piles exhibit an overall uplift trend, with the piles near the east abutment slightly less lifted than other locations. As the bored cast-in-situ piles are constructed in the water, they are subject to river flow and tide effects. Moreover, during the construction of bored cast-in-situ piles, uneven force on the foundation of grouting piles can occur due to the pouring pressure, leading to the uplift phenomenon.

4.3 Temperature Sensitivity Analysis of Time-series Deformation

Figure 5 displays the trend of time, deformation, and temperature at different locations of the under-construction bridge. The bridge abutment-bearing construction period was January-February 2022, while July-September 2022 marked an important stage in the construction of the main bridge. During the construction process, the force of the construction operations or the impact of external loads can affect the completed part of the bridge, resulting in significant deformation (Qin et al.2019).

Figure 5(a) shows that the deformation of the east approach span is similar to the temperature trend from March to June. It exhibits a vibration of plus or minus 5 mm from February to March and experiences a sudden uplift of 15 mm in July, which is likely influenced by the construction of the main bridge. Figure 5(b) reveals that the deformation of the west approach span shows random vibration and is not significantly related to the temperature trend.

Figure 5(c) demonstrates that the deformation of the west abutment is opposite to the temperature trend from November 2021 to February 2022. The deformation from March to July is consistent with the temperature trend, and the uplift in July is not significantly related to the temperature change. Figure 5(d) shows that the deformation of the east abutment is similar to the temperature trend from April to July 2022 but opposite to the temperature trend from July to September. Finally, Figure 5(e) indicates that the bored cast-in-situ piles exhibit high agreement with the temperature trend from February to June 2022, but do not show high sensitivity to temperature at other times.

From an overall perspective, the under-construction bridge exhibited a relatively obvious uplift at different locations of the bridge body in January, April, and July 2022. The deformation observed in January 2022 may be related to the construction of the abutment area, and may not be sensitive to temperature changes. In April, the under-construction bridge body was relatively stable, and the deformation trend was more consistent with temperature changes. In July, the deformation may be related to the construction of the main bridge, and the temperature is generally higher in summer, so temperature changes may not be a decisive factor for the deformation of the under-construction bridge.

5. CONCLUSION

In this study, the PS point identification method called the Three-Threshold Joint Algorithm (TTJA), which combines the amplitude dispersion index, statistical median of amplitude mean, and temporal coherence coefficient, was used to monitor the deformation of the under-construction bridge over the JingXiong Expressway-Yongding River. The findings of the study are as follows:

(1) The TTJA method produced high-quality PSs. The joint point identification method combines the advantages of amplitude dispersion stability and temporal coherence, and the extracted PS points not only cover the important main part of the under-construction bridge but also have a more uniform point distribution. Additionally, the method removes some error points such as water body shadow and noise. The number of candidate points increased by 14% compared to the ADI method and 10% compared to the CCT method.

(2) The deformation trend of the under-construction bridge over the JingXiong Expressway-Yongding River and the surrounding area was determined. Based on the deformation rate of the under-construction bridge and the surrounding area, it can be seen that the subsidence rate of the bridge body and the surrounding area during the monitoring period was within a reasonable range, with a deformation rate ranging from -15 to 20 mm/year. Overall, the trend shows subsidence in the west and uplift in the east. The main body of the bridge is relatively stable, but the deformation of the bored cast-in-situ piles and the connection between the approach span and the abutment is more prominent than in other areas. These areas require careful monitoring and prevention in subsequent stages.

(3) The structural deformation of the under-construction bridge is related to the ambient temperature, and different structural locations exhibit varying sensitivity to temperature. The correlation between the deformation trend of the west abutment, east approach span, and bored cast-in-situ piles is high. However, the correlation is not apparent in the early stage of the east abutment, and the overall correlation with temperature is not evident in the west approach span.

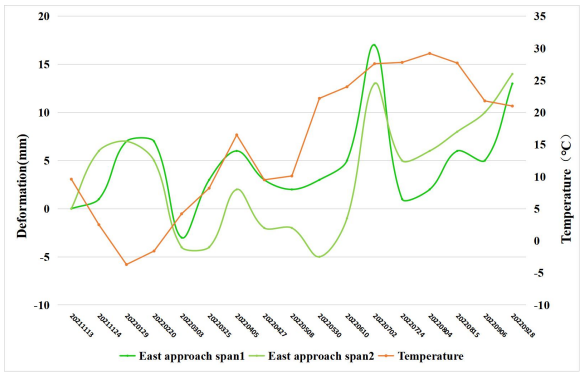

Figure 5(a). East approach span time series deformation and temperature trend result

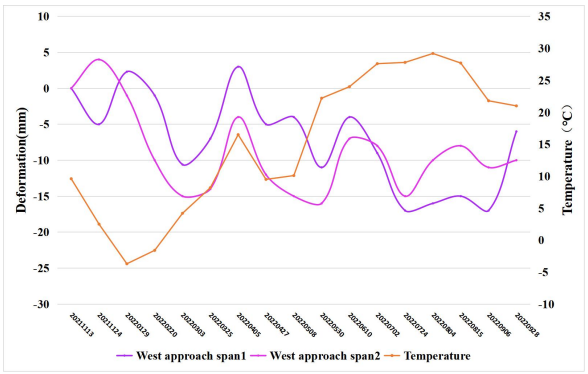

Figure 5(b). West approach span time series deformation and temperature trend result

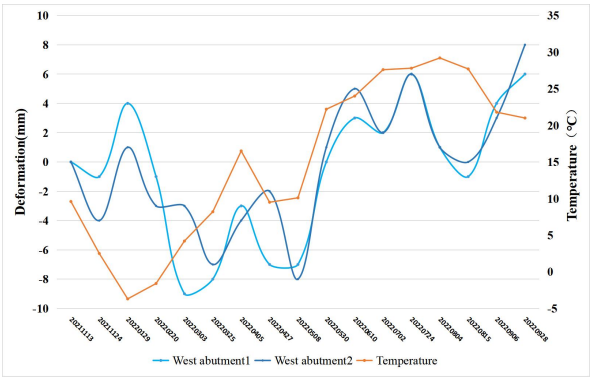

Figure 5(c). West abutment time series deformation and temperature trend result

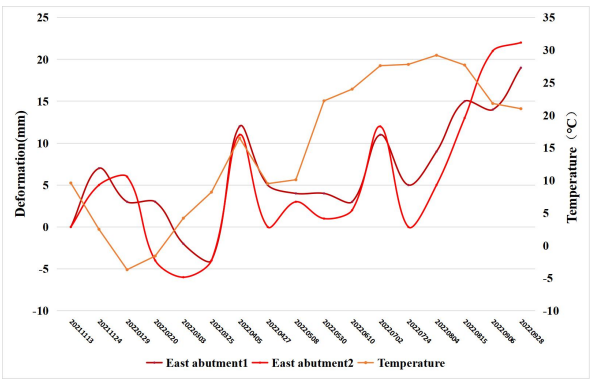

Figure 5(d). East abutment time series deformation and temperature trend result

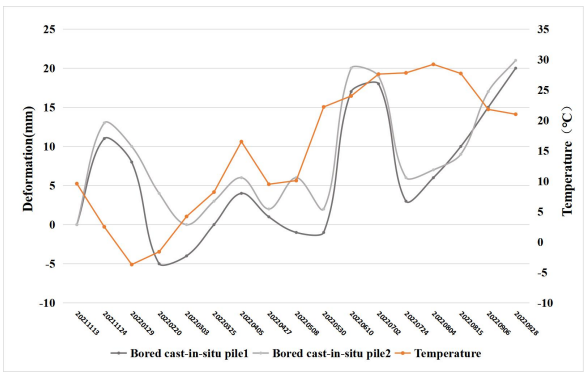

Figure 5(e). Bored cast-in-situ piles time series deformation and temperature trend result

ACKNOWLEDGMENTS

This study was supported by grants from the following projects: Beijing Key Laboratory of Urban Spatial Information Engineering (NO. 20230101), Beijing Higher Education Undergraduate Teaching Reform and Innovation Project (NO. 202110016004) and Beijing Education Science Planning Project (NO. CDDB21191).

REFERENCES

Galvão, N., Matos, J. C., & Oliveira, D. V. (2021). Human Error–Induced Risk in Reinforced Concrete Bridge Engineering. *Journal of Performance of Constructed Facilities*, *35*(4), 04021026.

Ge, D., Zhang, L., Li, M., Liu, B., & Wang, Y. (2016, July). Beijing subway tunnelings and high-speed railway subsidence monitoring with PSInSAR and TerraSAR-X data. In *2016 IEEE International Geoscience and Remote Sensing Symposium (IGARSS)* (pp. 6883-6886). IEEE.

Cusson, D., Trischuk, K., Hébert, D., Hewus, G., Gara, M., & Ghuman, P. (2018). Satellite-based InSAR monitoring of highway bridges: validation case study on the North Channel Bridge in Ontario, Canada. *Transportation Research Record*, *2672*(45), 76-86.

Farneti, E., Cavalagli, N., Costantini, M., Trillo, F., Minati, F., Venanzi, I., & Ubertini, F. (2023). A method for structural monitoring of multispan bridges using satellite InSAR data with uncertainty quantification and its pre-collapse application to the Albiano-Magra Bridge in Italy. *Structural Health Monitoring*, *22*(1), 353-371.

Ferretti, A., Prati, C., & Rocca, F. (2000). Nonlinear subsidence rate estimation using permanent scatterers in differential SAR interferometry. *IEEE Transactions on geoscience and remote sensing*, *38*(5), 2202-2212.

Ferretti, A., Prati, C., & Rocca, F. (2001). Permanent scatterers in SAR interferometry. *IEEE Transactions on geoscience and remote sensing*, *39*(1), 8-20.

Navneet, S., Kim, J. W., & Lu, Z. (2017). A new InSAR persistent scatterer selection technique using top eigenvalue of coherence matrix. *IEEE Transactions on Geoscience and Remote Sensing*, *56*(4), 1969-1978.

Zhou, Di, et al. "Integrating RELAX with PS-InSAR technique to improve identification of persistent scatterers for land subsidence monitoring." *Remote Sensing* 12.17 (2020): 2730.

Pierluigi Confuorto, et al. "Post-failure evolution analysis of a rainfall-triggered landslide by multi-temporal interferometry SAR approaches integrated with geotechnical analysis." *Remote sensing of environment* 188 (2017): 51-72.

Lazecky, M., Perissin, D., Bakon, M., de Sousa, J. M., Hlavacova, I., & Real, N. (2015, March). Potential of satellite InSAR techniques for monitoring of bridge deformations. In *2015 Joint Urban Remote Sensing Event (JURSE)* (pp. 1-4). IEEE.

Schlögl, M., Widhalm, B., & Avian, M. (2021). Comprehensive time-series analysis of bridge deformation using differential satellite radar interferometry based on Sentinel-1. *ISPRS Journal of Photogrammetry and Remote Sensing*, *172*, 132-146.

Lyu, M., Ke, Y., Li, X., Zhu, L., Guo, L., & Gong, H. (2020). Detection of seasonal deformation of highway overpasses using the PS-InSAR technique: A case study in Beijing urban area. *Remote Sensing*, *12*(18), 3071.

Luo, X., Huang, D., Liu, G. Automated Detection of Permanent Scatterers in Time Serial Differential Radar Interferometry (in Chinese), *J. Southwest Jiaotong Univ.*, 42 (2007), 414–418

Liu, W., Zhang, Q., & Zhao, Y. (2020). A fuzzy identification method for persistent scatterers in PSInSAR technology. *Mathematical Biosciences and Engineering*, *17*(6), 6928-6944.

Luo, X. G., Wang, J., Xu, Z., Zhu, S., Meng, L., Liu, J., & Cui, Y. (2018). Dynamic analysis of urban ground subsidence in Beijing based on the permanent scattering insar technology. *Journal of Applied Remote Sensing*, *12*(2), 026001-026001.

Natsuaki, R., Nagai, H., Tomii, N., & Tadono, T. (2018). Sensitivity and limitation in damage detection for individual buildings using InSAR coherence—A case study in 2016 Kumamoto earthquakes. *Remote Sensing*, *10*(2), 245.

Jung, J., Kim, D. J., Lavalle, M., & Yun, S. H. (2016). Coherent change detection using InSAR temporal decorrelation model: A case study for volcanic ash detection. *IEEE Transactions on Geoscience and Remote Sensing*, *54*(10), 5765-5775.

Delgado Blasco, J. M., Foumelis, M., Stewart, C., & Hooper, A. (2019). Measuring urban subsidence in the Rome metropolitan area (Italy) with Sentinel-1 SNAP-StaMPS persistent scatterer interferometry. *Remote Sensing*, *11*(2), 129.

Qin, X., Ding, X., Liao, M., Zhang, L., & Wang, C. (2019). A bridge-tailored multi-temporal DInSAR approach for remote exploration of deformation characteristics and mechanisms of complexly structured bridges. *ISPRS Journal of Photogrammetry and Remote Sensing*, *156*, 27-50.